HHS Public Access

Author manuscript

Exp Hematol. Author manuscript; available in PMC 2024 February 04.

Published in final edited form as:

Exp Hematol. 2021 April ; 96: 44–51. doi:10.1016/j.exphem.2021.01.005.

Proteoglycans regulate protein tyrosine phosphatase receptor - sigma organization on hematopoietic stem/progenitor cells

Christina M. Termini[1,2,3], **Amara Pang**[1,3], **Destiny M. Batton**[1], **John P. Chute**[1,2,3,4,5]

[1]Division of Hematology/Oncology, Department of Medicine, UCLA

[2]Department of Orthopaedic Surgery, UCLA

[3]Department of Medicine, Cedars Sinai Medical Center, Los Angeles, CA

[4]Broad Stem Cell Research Center, UCLA

[5]Jonsson Comprehensive Cancer Center, UCLA

Abstract

Receptor protein tyrosine phosphatase receptor - sigma (PTPσ) is highly expressed by murine and human hematopoietic stem cells (HSCs) and negatively regulates HSC self-renewal and regeneration. Previous studies of the nervous system suggest that heparan sulfate proteoglycans can inactivate PTPσ by clustering PTPσ receptors on neurons, but this finding has yet to be visually verified with adequate resolution. Here, we sought to visualize and quantify how heparan sulfate proteoglycans regulate the organization and activation of PTPσ in hematopoietic stem/progenitor cells (HSPCs). Our study demonstrates that Syndecan-2 promotes PTPσ clustering, which sustains Phospho-Tyrosine and Phospho-Erzin levels in association with augmentation of hematopoietic colony formation. Strategies that promote clustering of PTPσ on HSPCs may serve to powerfully augment hematopoietic function.

Keywords

hematopoietic stem cells; protein tyrosine phosphatase receptor - sigma; molecular organization; super-resolution microscopy

Introduction

Hematopoietic stem cell transplantation is utilized in the curative therapy of thousands of patients with hematologic malignancies and blood dyscrasias annually [1]. In the United

Corresponding Author: John P. Chute M.D., Chief, Division of Hematology, Associate Director, Regenerative Medicine Institute , Cedars Sinai Medical Center, Phone: 310-248-7622 , john.chute@cshs.org , Address: 8700 Beverly Boulevard ASHP A8700, Los Angeles, CA 90048-1860.

Author contributions

Project conceptualization was by CMT and JPC; experiments and analysis were performed by CMT and AP; CMT made the figures and the graphical abstract; CMT and JPC wrote the paper with input from all authors.

Category: Normal hematopoiesis

Declaration of interests

The authors declare no competing financial interests.

States, only 16 – 75% of all patients who meet an indication for an allogeneic HSC transplant will have an HLA-matched sibling or matched unrelated donor available [2]. In such patients, alternative donor HSC transplantation can be performed, utilizing either human cord blood or haploidentical related donors [3–8]. In both cord blood transplantation and haploidentical donor transplantation, HSC dose is associated with improved outcomes, whereas insufficient HSC doses are associated with poor outcomes [9, 10]. Improved understanding of the basic mechanisms that regulate HSC self-renewal and function could provide the foundation for methods to better optimize HSC grafts for transplantation.

We previously discovered that the proteoglycan-binding receptor, PTPσ, is differentially expressed by murine and human HSCs and functions as a negative regulator of HSC self-renewal [11]. PTPσ – deficient murine HSCs and PTPσ(−) human CB HSCs display significantly increased in vivo multilineage repopulating capacity compared to PTPσ(+) HSCs [11]. In subsequent studies, we demonstrated that systemic administration of a selective, allosteric PTPσ inhibitor promoted murine HSC regeneration after total body irradiation or myelosuppressive chemotherapy via augmentation of Rac1 activity [12]. Given the crucial role of PTPσ in regulating HSC function, methods to target PTPσ could have therapeutic potential for human hematopoietic regeneration.

Previous studies have demonstrated that Syndecans, which are heparan sulfate proteoglycans, can bind to PTPσ, to regulate downstream cellular signaling [13, 14]. For example, Syndecan-4 binds to PTPσ, expressed on the surface of fibroblast-like synoviocytes, thereby inactivating PTPσ and modulating cytoskeletal function [14]. Additional studies showed that heparan sulfates cluster PTPσ to promote neuronal extension, while chondroitin sulfates de-aggregate PTPσ, thereby inhibiting neuronal growth [13]. Inactivation of PTPσ also promotes regeneration after spinal cord injury [15–17]. Given the recently discovered role of PTPσ in regulating HSC function, we utilized stimulated emission depletion (STED) super-resolution imaging to visualize how proteoglycans regulate the organization of PTPσ on HSCs with nanoscale resolution. We determined that recombinant proteoglycans regulate the organization of PTPσ on the surface of HSPCs, resulting in increased levels of phospho-tyrosine and phospho-Ezrin expression, and augmented hematopoietic progenitor colony growth. These data demonstrate the mechanistic role of proteoglycans in regulating PTPσ structure and function on HSCs and the attendant impact on hematopoietic progenitor cell growth.

Methods

Mice

All mouse procedures were performed in accordance with Animal Use Protocol #2014–021-21 (Principal Investigator, John Chute), approved by the UCLA Animal Care and Use Committee. All mice were housed and maintained in the UCLA Radiation Oncology vivarium. For all experiments, 8–12-week-old mixed gender adult mice were used.

Fluorescence Activated Cell Sorting (FACS)

Bone marrow (BM) was isolated from the tibia and femurs of adult C57BL/6 mice (The Jackson Laboratory, Bar Harbor, ME, JAX: 000664) by flushing bones with IMDM (ThermoFisher, Waltham, MA 12440053) + 5% FBS (GE Healthcare, Chicago IL), 1% penicillin/streptomycin (ThermoFisher, Waltham, MA) (Complete IMDM). Cells were resuspended in ACK buffer (ThermoFisher, Waltham, MA) for red blood cell lysis. Cells were prepared for lineage depletion based upon the manufacturer's protocol (Miltenyi Biotec, Auburn, CA) and Lin^- cells were stained with antibodies to Lineage (BD Biosciences, 561301), c-Kit (BD Biosciences, 553355), and Sca-1 (BD Biosciences, 560654) for 30 minutes. Cells were washed, filtered and stained with 7AAD (BD Biosciences, 559925) before sorting on a BD FACSAria. Compensation controls were utilized to set voltages and sort gating was set according to unstained and isotype stained samples. Cells were sorted into Complete IMDM supplemented with thrombopoietin (20 ng/ml, R&D Systems, 488-TO/CF), flt-3 ligand (50 ng/ml, R&D Systems, 427-FL/CF), and stem cell factor (150 ng/ml, R&D Systems, 455-MC/CF)(TSF media).

Cell culture and treatment

Glass bottom dishes (35 mm, MatTek Corporation, Ashland, MA P35G-0.170–14-C) were coated with fibronectin (Millipore Sigma, Burlington, MA, 341635–1MG) at 25 ug/ml in PBS for 20 minutes. 1×10^4 sorted cells were plated on fibronectin coated slides. Cells were cultured for 16 hours in a humidified incubator (5% CO_2, 37 degrees) and then serum-starved in IMDM for 30 minutes. Syndecan-2 (R&D, 6585-SD-050), Syndecan-4 (R&D, 6267-SD-050), Biglycan (R&D, 8128-CM-050), and Glypican-6 (R&D, 9429-GP-050) were reconstituted according to the manufacturer's protocol. Non-adherent cells and the supernatant were gently removed from the slide using a micropipette. The media was replaced with 20 ug/mL of recombinant proteoglycan dissolved in TSF media and cells were cultured for 30 minutes.

Immunostaining

For immunostaining, non-adherent cells and the supernatant were gently removed using a micropipette. The slide was washed using PBS and then the cells were fixed using 4% paraformaldehyde (Fisher Scientific, Waltham, MA, 50-980-487) for 20 minutes at room temperature. Following fixation, cells were washed once for 5 minutes using PBS. The cells were permeabilized using 0.5% Trition-X-100 dissolved in 1x PBS for 30 minutes at room temperature and then washed once. Cells were then blocked for 30 minutes (0.5% Trition-X-100 with 5% FBS). Cells were then stained by diluting primary antibody in blocking buffer and staining for 1 hour covered. Unconjugated primary antibodies used were PTPσ antibody (MyBioSource, MBS#9129086, 1:100, San Diego, CA) and Ezrin (ThermoFisher, MA5-13862, 1:200). Cells were then washed twice and incubated with secondary antibody (Anti-rabbit, Atto-647N, 40839-1ML-F 1:200, Sigma-Aldrich, or anti-mouse Alexa Fluor Plus 488 IgG, ThermoFisher, A32723, 1:200, Waltham, MA) and/or directly conjugated phospho-Tyrosine Alexa Fluor 488 (Biolegend, #309306, 1:200, San Diego, CA). Cells were stained for 1 hour and covered. The slides were washed twice and post-label fixed with 4% PFA for 10 minutes. The sample was then rinsed once with PBS. The slide was

mounted with Prolong Gold (ThermoFisher, Waltham, MA, P36930), dried overnight at 4 degrees, and covered. Cells were prepared using the same technique for confocal staining and stained using a phospho-Ezrin antibody (Abcam, cat# ab47273, 1:200) followed by secondary anti-rabbit IgG Alexa Fluor 488 (ThermoFisher, A21206, 1:200).

Confocal and STED Imaging

The following day, samples were imaged using a Leica SP8 (DMI8-CS) microscope system. 1376 × 1376 px images were acquired in 8-bit mode using a HC PL APO CS2 100x/1.40 oil objective lens. White light laser lines were set to 488 nm and 633 nm for excitation and 592 nm and 775 nm for depletion, respectively. Sequential STED was performed using bidirectional x scanning (speed at 600) and the STED delay time offset was set according to each day of imaging. Cells were selected at random, with the user first identifying cells in brightfield mode before initiating confocal or STED imaging. Deconvolution was performed using Huygens Array Detector deconvolution software (Carl Zeiss Microscopy, Oberkochen, Germany) with the mounting media refractive index matched for Prolong Gold mounting media.

Image analysis

For IMARIS analysis, a 300 × 300 pixel square within the center of each cell was analyzed for PTPσ domain size using the analyze surface function. The absolute intensity threshold of 1.2×10^4 (absolute intensity) and 10 voxels was used with no smoothing. Co-localization analysis was performed using the Just Another Colocalization Plugin (JACoP) in ImageJ to calculate the Pearson's and Manders' coefficients. For MFI analysis, the image was opened in ImageJ and the measure tool was used to calculate the MFI.

Cell Migration

TransWell plates with 3 um membranes (FisherScientific # 07-200-148) were coated with fibronectin (25ug/ml) for 2 hours prior to adding 2×10^5 mouse bone marrow cells resuspended in TSF media to the top chamber. Cells were allowed to migrate to media or media supplemented with SDF-1 (500 mg/mL, R&D Technology, Cat# 460-SD-050/CF) for 16 hours, at which point the cells in the bottom well were counted. Percent migration was determined by dividing the number of cells in the bottom well by the number of cells input (2×10^5).

Colony forming cell assay

Sorted BM c-kit$^+$sca-1$^+$lineage$^-$ (KSL) hematopoietic stem/progenitor cells were resuspended in TSF enriched to give a final concentration of 20 μg/mL Syndecan-2 (R&D, 6585-SD-050) 1 μg/mL DJ001, 1 ug/ml PTPRS antibody (MyBioSource, MBS#9129086), 10 μM NSC668394 (Sigma Aldrich, #341216-10MG), or a combination of the above conditions. Colonies were counted on day 8 after plating. DJ001 was synthesized at the University of California, Los Angeles as previously described [12].

Statistical Analysis

All statistical analyses were performed using GraphPad Prism (GraphPad Software, San Diego, CA, Ver 8.4.3). For all analyses, * $p < 0.05$, ** $p < 0.01$, *** $p < 0.001$, **** $p < 0.0001$. For individual comparisons, student's unpaired t-test was used. For multiple comparisons, Holm-Sidak corrected t-test was used after one-way ANOVA. Outliers were identified using Grubbs' outlier test with alpha = 0.05.

Results and Discussion

We developed an experimental pipeline enabling us to visualize the nanoscale organization of PTPσ on murine BM HSPCs (Fig. 1A). We first used FACS to isolate BM KSL HSPCs from adult mice (Fig. 1B). One of the challenges of imaging HSPCs is their non-adherent properties, which can lead to sample drift during the course of imaging. To circumvent this concern, we immobilized HSPCs on fibronectin-coated slides according to previously described super-resolution imaging studies of non-adherent cells [18], as fibronectin can regulate HSPC migration [19]. While conventional microscopy has provided insight regarding the cellular localization of heparan sulfates and PTPσ in prior studies using mouse dorsal root ganglion neuron cultures [13], the diffraction limit (~200 nm when using confocal microscopy) has inhibited the capacity to visualize how PTPσ organization is regulated by proteoglycans at the nanoscale. We have utilized the super-resolution microscopy technique, STED [20–22], which in our studies has a resolution of < 50 nm, to provide the resolution necessary to discern subtle changes in the molecular organization of PTPσ. BM KSL cells were plated on glass slides, stimulated with Syndecan-2, Syndecan-4, Glypican-6, or Biglycan and stained. Samples were first imaged using a confocal microscope system (Fig. 1C), which enables visualization of the overall staining pattern at lower magnification. We next imaged our samples using a STED microscope system, which enables visualization of nanoscale PTPσ organization with improved resolution compared to confocal microscopy (Fig. 1D, E). To further assess this improvement in resolution, we analyzed the molecular localization of PTPσ and Phospho-Tyrosine residues using confocal microscopy and STED (Fig. 1F, G). While line-scan analyses demonstrated similar fluorescence profiles of PTPσ and Phospho-Tyrosine (Fig. 1H, I), we detected a significant reduction in the molecular co-localization of these proteins using STED based on Pearson's (Fig. 1J) and Manders' analysis (Fig. 1K). Taken together, these data demonstrate how increased resolution from STED imaging influences the apparent molecular co-localization detected between proteins in HSPCs.

We next utilized STED microscopy to quantify how proteoglycan treatment regulates the molecular organization of PTPσ on BM KSL cells (Fig. 2A-G). We first confirmed staining specificity of PTPσ and phospho-Tyrosine antibodies using STED (Fig. 2A, B). We next visualized the molecular arrangement of PTPσ microdomains in the presence and absence of Syndecan-2, Syndecan-4, Glypican-6 and Biglycan using STED images after deconvolution (Fig. 2C-G), which we quantified using IMARIS. We detected a significant increase in PTPσ domain area upon treatment with recombinant Syndecan-2 (Fig. 2D, H). Meanwhile, treatment with Syndecan-4 or Glypican-6 did not alter PTPσ domain area (Fig. 2E, F, H). We also treated cells with Biglycan, a chondroitin sulfate proteoglycan enriched in HSCs at

the genetic level [23]. Biglycan treatment did not change PTPσ domain area compared to controls (Fig. 2G, H). We also analyzed how proteoglycan treatment regulated the distribution of PTPσ domains using frequency distribution analysis. Syndecan-2 treatment significantly increased the proportion of large PTPσ clusters compared to control treatment and treatment with other proteoglycans (Fig. 2I). Time course analyses demonstrate that the increase in PTPσ domain size by Syndecan-2 occurs within 5 minutes and is sustained through 20 minutes post-treatment, while no longer detected at 1 hour post-Syndecan-2 treatment (Fig. 2J). Taken together, these data suggest Syndecan-2 treatment oligomerizes PTPσ on HSPCs.

Upon clustering, PTPσ is deactivated, which diminishes substrate dephosphorylation [13]. We used two-color STED imaging to quantify the molecular co-localization of Phospho-Tyrosine residues relative to PTPσ. We did not detect a change in the molecular co-localization of PTPσ with Phospho-Tyrosine upon proteoglycan treatment (Fig. 2A-G, 2K), suggesting that Syndecan-2 did not change the capacity for PTPσ to localize with Phospho-Tyrosine residues. Interestingly, quantification of the Phospho-Tyrosine levels revealed that Syndecan-2 treatment increased Phospho-Tyrosine expression, consistent with deactivation of PTPσ (Fig. 2L).

Since proteoglycans can change the migratory behavior of non-hematopoietic cells and hematopoietic cells [19, 24], we tested whether Syndecan-2 treatment could affect BM cell migration in vitro. We observed no change in BM cell migration at baseline or in response to an SDF-1 gradient (Fig. 3A). Recent studies have demonstrated that Ezrin, a critical regulator of the actin cytoskeleton, is a substrate for PTPσ in mouse intestinal tissue [25–27]. To analyze the potential relationship between Syndecan-2 - mediated clustering of PTPσ and Ezrin activation in BM HSPCs, we used quantitative confocal microscopy. We detected a significant increase in Phospho-Ezrin expression in BM KSL cells immediately following Syndecan-2 treatment (Fig. 3B-F). For comparison, we also treated BM KSL cells with DJ001, a specific allosteric inhibitor of PTPσ. DJ001 treatment also significantly increased Phospho-Ezrin expression in HSPCs (Fig. 3E, F). STED imaging of Ezrin and PTPσ revealed no change in the localization of PTPσ and Ezrin upon Syndecan-2 treatment, suggesting that Syndecan-2 inactivates PTPσ but does not change the localization of the receptor relative to substrate (Fig. 3G-I). These data suggest that Syndecan-2 promotes PTPσ clustering on HSPCs, thereby inactivating PTPσ and augmenting Ezrin activation.

To analyze the functional consequence of Syndecan-2-mediated clustering of PTPσ, we analyzed BM hematopoietic colony formation. We observed a significant increase in total, granulocyte/monocyte (GM) and granulocyte, erythrocyte, monocyte, megakaryocyte (GEMM) hematopoietic colony formation in response to Syndecan-2 treatment of BM KSL cells (Fig. 3J-L). Interestingly, the combined treatment of BM KSL cells with Syndecan-2 plus the PTPσ inhibitor, DJ001, had no additive effect on hematopoietic colony formation (Fig. 3J-L), suggesting that both Syndecan-2 and DJ001 were working through the same mechanism. In contrast, inhibition of Ezrin using small molecule, NSC668394 [28], prevented the Syndecan-2 - mediated increase in hematopoietic colony formation (Fig. 3J-L). Taken together, these data suggest Syndecan-2 promotes hematopoietic progenitor function by clustering PTPσ, which in turn increases Phospho-Ezrin levels. We hypothesize

that Ezrin activation may regulate hematopoietic cell proliferation since Ezrin has been shown to promote the proliferation of cervical cancer cells, pancreatic cancer cells, and endothelial cells [29–31]. Our future studies will evaluate the underlying role of Ezrin in HSPC function and the mechanism through which Syndecan-2 regulates Ezrin-mediated adhesion, migration and signaling in HSPCs. In summary, Syndecan-2 - mediated rearrangement of PTPσ on HSPC membranes reduces PTPσ activity, thereby increasing tyrosine phosphorylation and Ezrin activation in HSPCs. Modulation of PTPσ cell surface organization has important consequences for HSPC growth.

Acknowledgments

This work was supported by funding from NIAID AI067769 (JPC) and the Damon Runyon Cancer Foundation DRG-2327-18 (CMT), the Burroughs Wellcome Fund PDEP #1018686 (CMT), the UC President's Postdoctoral Fellowship (CMT). We acknowledge the generous technical support of Jeffrey Calimlim, Felicia Codrea, and Jessica Scholes of the UCLA Broad Stem Cell Center Flow Cytometry Facility and Liman Zhao for animal colony management. All microscopy was performed at the Advanced Light Microscopy/Spectroscopy Laboratory and the Leica Microsystems Center of Excellence at the California NanoSystems Institute at UCLA, with funding support from NIH Shared Instrumentation Grant S10OD025017 and NSF Major Research Instrumentation grant CHE-0722519. We thank Dr. Laurent Bentolila and Dr. Matthew Shibler for assistance with imaging.

References

1. D'Souza A, et al. , Current Use of and Trends in Hematopoietic Cell Transplantation in the United States. Biology of Blood and Marrow Transplantation, 2020. 26(8): p. E177–E182. [PubMed: 32438042]
2. Gragert L, et al. , HLA match likelihoods for hematopoietic stem-cell grafts in the U.S. registry. N Engl J Med, 2014. 371(4): p. 339–48. [PubMed: 25054717]
3. Copelan EA, Medical progress: Hematopoietic stem-cell transplantation. New England Journal of Medicine, 2006. 354(17): p. 1813–1826. [PubMed: 16641398]
4. Eapen M, et al. , Effect of graft source on unrelated donor haemopoietic stem-cell transplantation in adults with acute leukaemia: a retrospective analysis. Lancet Oncol, 2010. 11(7): p. 653–60. [PubMed: 20558104]
5. Eapen M, et al. , Outcomes of transplantation of unrelated donor umbilical cord blood and bone marrow in children with acute leukaemia: a comparison study. Lancet, 2007. 369(9577): p. 1947–54. [PubMed: 17560447]
6. Kurtzberg J, et al. , Placental blood as a source of hematopoietic stem cells for transplantation into unrelated recipients. New England Journal of Medicine, 1996. 335(3): p. 157–166. [PubMed: 8657213]
7. Laughlin MJ, et al. , Outcomes after transplantation of cord blood or bone marrow from unrelated donors in adults with leukemia. N Engl J Med, 2004. 351(22): p. 2265–75. [PubMed: 15564543]
8. Mehta RS, et al. , Composite GRFS and CRFS Outcomes After Adult Alternative Donor HCT. Journal of Clinical Oncology, 2020. 38(18): p. 2062-+. [PubMed: 32364845]
9. Cohen S, et al. , Hematopoietic stem cell transplantation using single UM171-expanded cord blood: a single-arm, phase 1–2 safety and feasibility study. Lancet Haematology, 2020. 7(2): p. E134–E145. [PubMed: 31704264]
10. Maffini E, et al. , CD34+cell dose effects on clinical outcomes after T-cell replete haploidentical allogeneic hematopoietic stem cell transplantation for acute myeloid leukemia using peripheral blood stem cells. A study from the acute leukemia working Party of the European Society for blood and marrow transplantation (EBMT). American Journal of Hematology, 2020. 95(8): p. 892–899. [PubMed: 32303111]
11. Quarmyne M, et al. , Protein Tyrosine Phosphatase-Sigma (PTP sigma) Regulates Hematopoietic Stem Cell Repopulating Capacity. Blood, 2014. 124(21).

12. Zhang YR, et al. , PTP sigma inhibitors promote hematopoietic stem cell regeneration. Nature Communications, 2019. 10.
13. Coles CH, et al. , Proteoglycan-specific molecular switch for RPTPsigma clustering and neuronal extension. Science, 2011. 332(6028): p. 484–8. [PubMed: 21454754]
14. Doody KM, et al. , Targeting phosphatase-dependent proteoglycan switch for rheumatoid arthritis therapy. Sci Transl Med, 2015. 7(288): p. 288ra76.
15. Dyck S, et al. , LAR and PTPsigma receptors are negative regulators of oligodendrogenesis and oligodendrocyte integrity in spinal cord injury. Glia, 2019. 67(1): p. 125–145. [PubMed: 30394599]
16. Dyck S, et al. , Perturbing chondroitin sulfate proteoglycan signaling through LAR and PTPsigma receptors promotes a beneficial inflammatory response following spinal cord injury. J Neuroinflammation, 2018. 15(1): p. 90. [PubMed: 29558941]
17. Dyck SM, et al. , Chondroitin Sulfate Proteoglycans Negatively Modulate Spinal Cord Neural Precursor Cells by Signaling Through LAR and RPTP sigma and Modulation of the Rho/ROCK Pathway. Stem Cells, 2015. 33(8): p. 2550–2563. [PubMed: 25703008]
18. Termini CM, Lidke KA, and Gillette JM, Tetraspanin CD82 Regulates the Spatiotemporal Dynamics of PKCalpha in Acute Myeloid Leukemia. Sci Rep, 2016. 6: p. 29859. [PubMed: 27417454]
19. Craddock CF, et al. , The role of CS1 moiety of fibronectin in VLA mediated haemopoietic progenitor trafficking. Br J Haematol, 1997. 97(1): p. 15–21. [PubMed: 9136937]
20. Hell SW and Kroug M, Ground-State-Depletion Fluorescence Microscopy - a Concept for Breaking the Diffraction Resolution Limit. Applied Physics B-Lasers and Optics, 1995. 60(5): p. 495–497.
21. Hell SW and Wichmann J, Breaking the Diffraction Resolution Limit by Stimulated-Emission - Stimulated-Emission-Depletion Fluorescence Microscopy. Optics Letters, 1994. 19(11): p. 780–782. [PubMed: 19844443]
22. Klar TA, et al. , Fluorescence microscopy with diffraction resolution barrier broken by stimulated emission. Proceedings of the National Academy of Sciences of the United States of America, 2000. 97(15): p. 8206–8210. [PubMed: 10899992]
23. Kiel MJ, et al. , SLAM family receptors distinguish hematopoietic stem and progenitor cells and reveal endothelial niches for stem cells. Cell, 2005. 121(7): p. 1109–21. [PubMed: 15989959]
24. Lee H, et al. , Syndecan-2 cytoplasmic domain regulates colon cancer cell migration via interaction with syntenin-1. Biochem Biophys Res Commun, 2011. 409(1): p. 148–53. [PubMed: 21569759]
25. Hiscox S and Jiang WG, Ezrin regulates cell-cell and cell-matrix adhesion, a possible role with E-cadherin/beta-catenin. Journal of Cell Science, 1999. 112(18): p. 3081–3090. [PubMed: 10462524]
26. McClatchey AI, ERM proteins at a glance. Journal of Cell Science, 2014. 127(15): p. 3199–3204. [PubMed: 24951115]
27. Murchie R, et al. , Protein tyrosine phosphatase sigma targets apical junction complex proteins in the intestine and regulates epithelial permeability. Proceedings of the National Academy of Sciences of the United States of America, 2014. 111(2): p. 693–698. [PubMed: 24385580]
28. Bulut G, et al. , Small molecule inhibitors of ezrin inhibit the invasive phenotype of osteosarcoma cells. Oncogene, 2012. 31(3): p. 269–81. [PubMed: 21706056]
29. Kishore R, et al. , The cytoskeletal protein ezrin regulates EC proliferation and angiogenesis via TNF-alpha-induced transcriptional repression of cyclin A (vol 115, pg 1785, 2005). Journal of Clinical Investigation, 2005. 115(10): p. 2955–2955.
30. Kong JN, et al. , Ezrin contributes to cervical cancer progression through induction of epithelial-mesenchymal transition. Oncotarget, 2016. 7(15): p. 19631–19642. [PubMed: 26933912]
31. Quan CJ, et al. , Ezrin promotes pancreatic cancer cell proliferation and invasion through activating the Akt/mTOR pathway and inducing YAP translocation. Cancer Management and Research, 2019. 11: p. 6553–6566. [PubMed: 31372056]

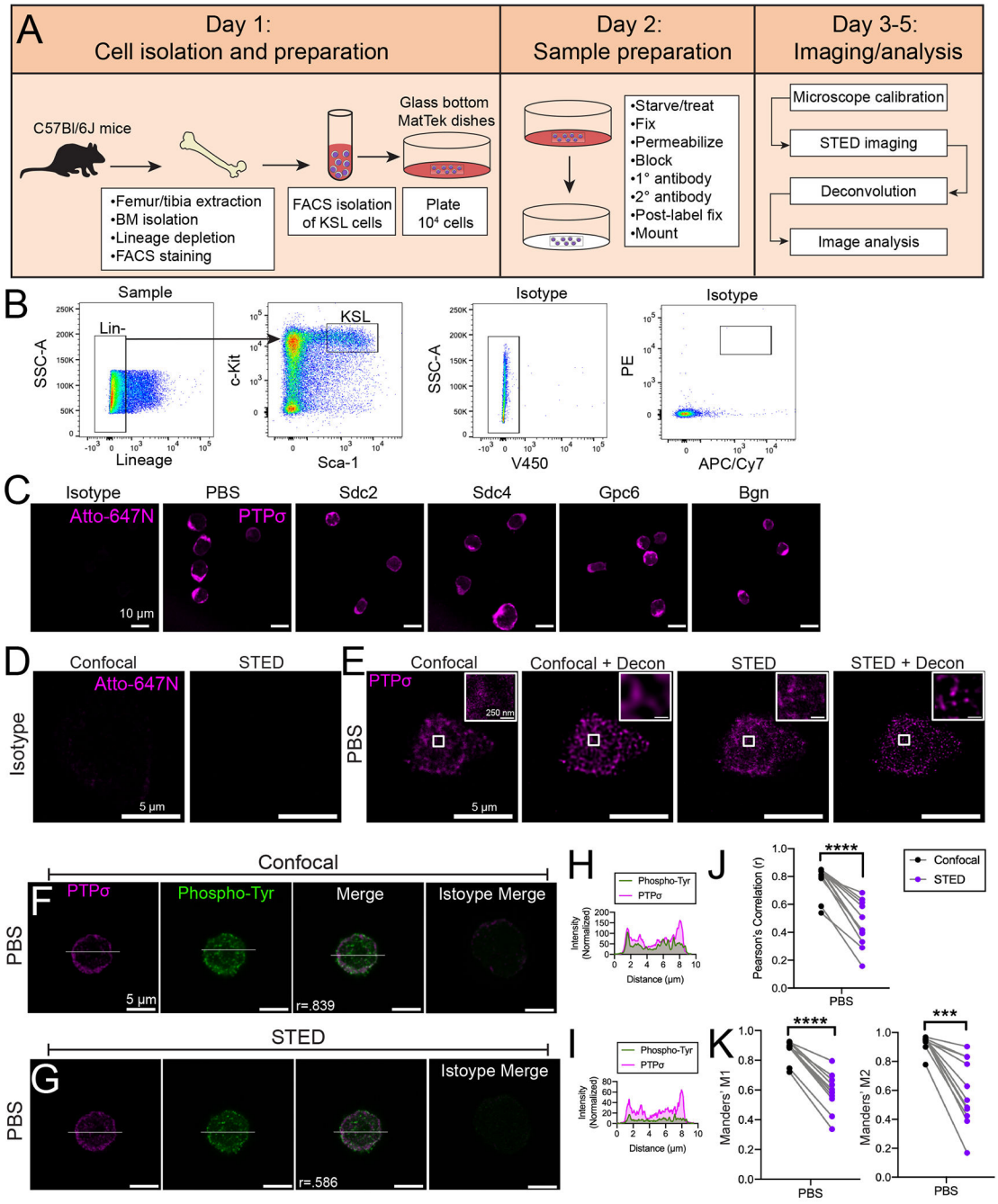

Figure 1: Super-resolution microscopy to analyze PTPσ localization on HSPCs.

(A) Experimental design used to isolate, prepare, and analyze BM KSL cells. (B) Representative gating for cell sorting strategy used to isolate murine HSPCs. (C) Representative confocal images taken using a 40X objective showing PTPσ distribution on HSPCs. Representative images showing (D) isotype controls or (E) PTPσ organization on HSPCs using confocal or STED microscopy, with and without deconvolution. Representative images and line-scan showing KSL cells imaged for PTPσ and Phospho-Tyrosine using (F) confocal and (G) STED microscopy without deconvolution. The

fluorescence profiles of PTPσ and Phospho-Tyrosine on cells imaged with (F) confocal and (G) STED are shown. Co-localization between PTPσ and Phospho-Tyrosine was quantified using (H) Pearson's correlation and (I) Manders' correlation analyses. (n=11 cells from 2 independent experiments using cells isolated from n=5 mice pooled, paired t-test). Images have been brightness and contrast enhanced equally for visualization purposes.

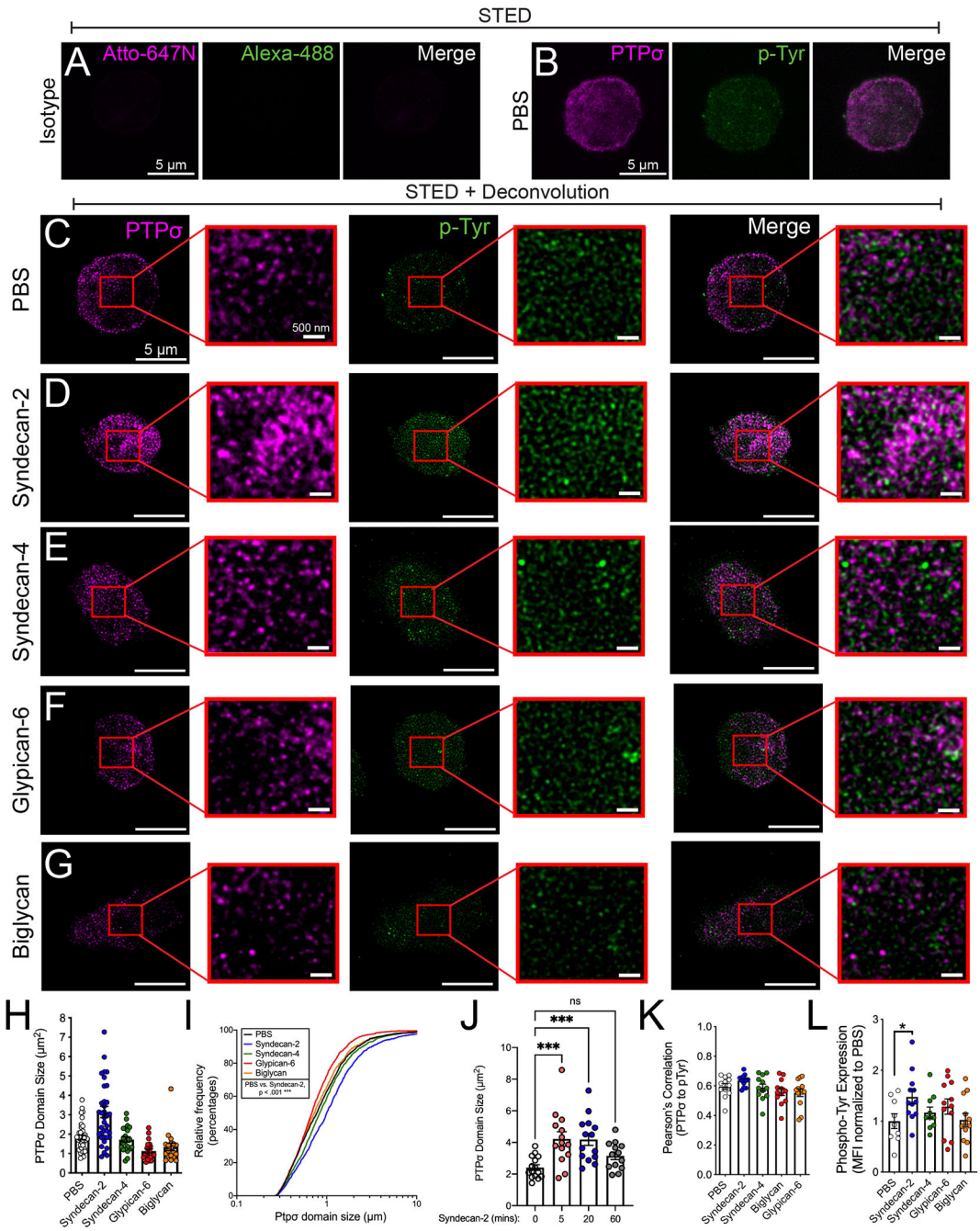

Figure 2: Syndecan-2 regulates PTPσ molecular organization and Phospho-Tyrosine levels in HSPCs.

STED imaging showing (A) isotype staining and (B) PTPσ and Phospho-Tyrosine in BM KSL cells treated with PBS. STED imaging with deconvolution of BM KSL cells treated with (C) PBS, (D) Syndecan-2, (E) Syndecan-4, (F) Glypican-6 or (G) Biglycan for 20 minutes. (H) PTPσ domain size was quantified using IMARIS software (n=19-22 cells/group from n=3 experiments using cells isolated from n=5 mice/pooled, statistics denote Holm-Sidak's multiple comparison t-test after one-way ANOVA). (I) PTPσ domain sizes are displayed as a cumulative distribution plot (n>1086 clusters/group from n=3 experiments

using cells isolated from n=5 mice/pooled, statistics denote Kolmogorov-Smirnov test of cluster cumulative distribution). (J) PTPσ domain size after Syndecan-2 treatment for 5, 20, and 60 minutes was quantified using IMARIS software (n=13-15 cells/group from n=2 experiments using cells isolated from n=5 mice/pooled, statistics denote Holm-Sidak's multiple comparison t-test after one-way ANOVA). (K) Co-localization analysis of PTPσ and Phospho-Tyrosine upon proteoglycan treatment (n=12-13 cells/group from n=2 experiments using cells isolated from n=5 mice/pooled). (L) Phospho-Tyrosine expression was quantified using ImageJ analysis for mean fluorescence intensity (MFI). MFI was normalized by dividing the MFI by the mean MFI of the PBS group to show expression relative to the PBS group. (n=9-12 cells/group from n=2 experiments using cells isolated from n=5 mice/pooled, statistics denote Holm-Sidak's multiple comparison t-test after one-way ANOVA). Error bars show S.E.M. Images have been brightness and contrast enhanced equally for visualization purposes.

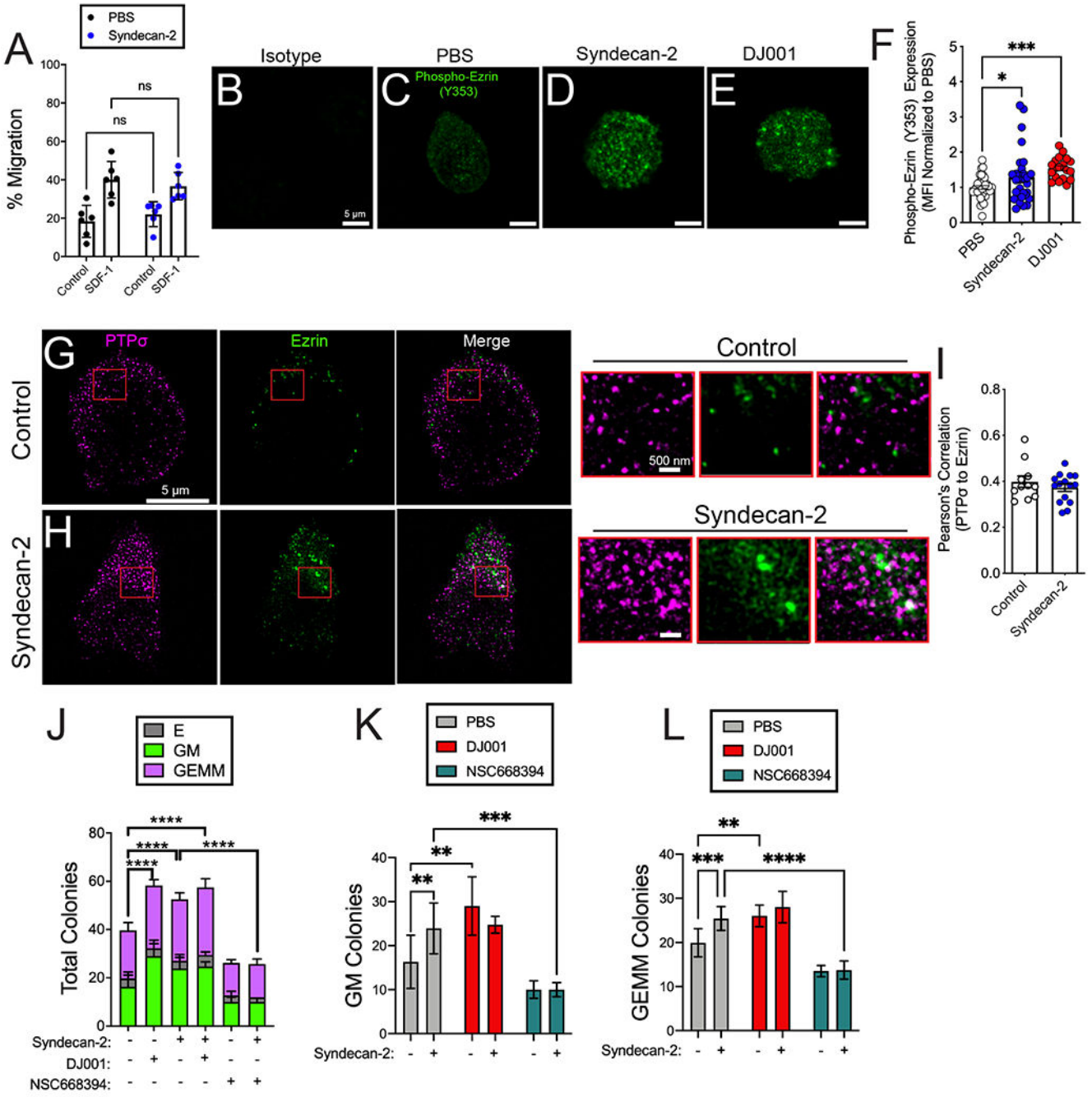

Figure 3: Syndecan-2 regulates Phospho-Ezrin levels in HSPCs.

(A) BM cell migration to control media or SDF-1 gradient after Syndecan-2 stimulation was quantified using TransWells. BM HSPCs were analyzed using confocal microscopy to visualize isotype control staining (B) and Phospho-Ezrin (Y353) staining after treatment with PBS (C), Syndecan-2 (D) or DJ001 (E). No deconvolution performed for images shown in B - E. (F) Phospho-Ezrin MFI was quantified from confocal images. MFI was normalized by dividing the MFI by the mean MFI of the PBS group to show expression relative to the PBS group. (n=19-36 cells/group from n=2 experiments using cells isolated from

n=5 mice/pooled, statistics show Holm-Sidak's multiple comparison t-test after one-way ANOVA). (G) STED imaging, with deconvolution, of PTPσ and Ezrin after control (PBS) or (H) Syndecan-2 treatment. (I) Pearson's correlation of PTPσ and Ezrin localization relative to one another (n=11-15 cells from n=2 experiments using cells isolated from n=5 mice/experiment, pooled). (J) Numbers of colony forming cells (colonies) are shown from BM KSL grown in the presence of Syndecan-2 (Sdc2) with or without blocking anti-PTPσ antibody or Ezrin inhibitor, NSC668394 for 7 days (n=3 experiments, n=4 replicates/experiment, cells sorted from n=5 mice/experiment, statistics show Holm-Sidak's multiple comparison t-test after one-way ANOVA). (K) Numbers of granulocyte, monocyte and (L) granulocyte, erythrocyte, monocyte, megakaryocyte colonies were quantified from BM KSL grown in the presence of Syndecan-2 (Sdc2) with or without blocking anti-PTPσ antibody or Ezrin inhibitor, NSC668394 for 7 days. (n=3 experiments, n=4 replicates/experiment, cells sorted from n=5 mice/experiment, statistics show Holm-Sidak's multiple comparison t-test after two-way ANOVA). Error bars denote S.E.M. Images have been brightness and contrast enhanced equally for visualization purposes.